Adv Syst Sci Appl 2024; **01**; 58-68
Published online at https://ijassa.ipu.ru.

Optimizing Mechanical Strength in W-30Cu/xTiC Alloys via Solid-State Sintering: A Comprehensive Characterization

Lahcene Mebarki[1*], Abdelyamine Boukhobza[2], Kamel Fedaoui[3], Lazhar Baroura[4], Ali Abderrazak Tadjeddine[2]

[1)] *Mechanics Research Center (CRM), Constantine, Algeria*

[2)] *LSETER Laboratory, Nour Bachir University Center, El-Bayadh, Algeria*

[3)] *LEREESI, Laboratory, HNS-RE2SD, Batna, Algeria*

[4)] *ISTA, University of Constantine 1, Algeria*

Abstract: The objective of this study is to investigate the influence of titanium carbide (TiC) on both the mechanical properties and microstructural characteristics of tungsten-copper (W-Cu) alloys. The manufacturing process adopted for this exploration employs solid-phase sintering, conducted at a temperature of 1,200°C under a uniaxial pressure of 30 MPa. This process is employed to synthesize W-30Cu/xTiC alloy powders, where 'x' denotes the weight percentages of 5, 10, and 15 for TiC. The alloys underwent a comprehensive analysis employing various analytical techniques to assess their mechanical and microstructural properties. These techniques include scanning electron microscopy (SEM), X-ray diffractometry (XRD), density evaluations, hardness tests, and flexural strength testing. Notably, the incorporation of titanium carbide (TiC) resulted in substantial improvements in both hardness and flexural strength, with the alloy containing 15% TiC exhibiting a microhardness value of 1420±5 HV0.1 and a flexural strength of 1745 N/mm². Additionally, the sintering process led to a significant increase in density, rising from 8.6g/cm³ to 13.8g/cm³. These findings underscore the positive impact of TiC and the sintering process on the alloy's mechanical and structural characteristics.

Keywords: WCu-TiC alloys, sintering, density, microhardness.

1. INTRODUCTION

Tungsten-based (W) alloys are renowned for their dual-phase structure, providing a favorable blend of hardness and ductility. Among these, W-Cu alloys are extensively used in electronic enclosures and heat sinks. However, the transformation of phases during sintering weakens the alloy's hardness [27]. This study aims to address this by exploring the addition of TiC to W-Cu alloys. The miscibility and uncreativeness between copper and tungsten pose challenges in their manufacturing, leading to the adoption of powder metallurgy methods [3]. The incorporation of TiC restricts the dissolution and precipitation of tungsten particles within the liquid copper phase, contributing to the prevention of phase growth during sintering [2].

Heavy tungsten-based (W) alloys exhibit a biphasic structure comprising a high-density body-centered cubic (BCC) phase and a face-centered cubic (FCC) phase, which offers a favorable combination of hardness and ductility [6]. Heavy tungsten-based alloys find applications in various industries, including aerospace, defense, medical, and nuclear fields, where their unique combination of properties is advantageous. These alloys are often used in situations where a balance of strength, radiation shielding, corrosion resistance, and hardness is crucial for optimal performance. Renowned for their exceptional mechanical properties, including high strength, radiation absorption capacity, resistance to wear and corrosion, as well

[*] Corresponding author: lahcenemebarki@yahoo.fr

as elevated hardness and density, these alloys find widespread utility across various industrial domains [10, 14]. Within this spectrum, W-Cu alloys have garnered substantial attention, notably in electronic enclosures and heat sinks for integrated circuits, owing to their compatibility with copper. Nonetheless, the susceptibility to the formation of a brittle CuW phase during sintering due to the disparate solubility of copper in tungsten poses a challenge, potentially compromising the hardness of W-Cu alloys [23, 5].

The adjustment of tungsten (W) and copper (Cu) ratios is a critical factor in leveraging the exceptional characteristics of both elements. However, challenges arise in the manufacturing of W-Cu alloys due to the immiscibility (limited ability to form a homogeneous mixture) and chemical inertness between copper and tungsten. These hurdles complicate the process of achieving a uniform distribution of the two elements in the alloy, impacting the alloy's overall properties and performance. Overcoming these challenges requires careful consideration and innovative approaches in alloy design and manufacturing processes to optimize the benefits of both tungsten and copper in the final material [4, 26]. Powder metallurgy methods such as infiltration melting, liquid phase sintering (LPS), and hot-pressing sintering (HPS) have been the recourse, augmented by the introduction of minute quantities of ceramic phases or rare earth oxide particles, enabling controlled recrystallization and enhanced dispersion [25, 7].

The process of augmenting tungsten-based alloys to enhance mechanical properties entails intentionally introducing specific elements such as nickel (Ni), cobalt (Co), iron (Fe), copper (Cu), and titanium carbide (TiC). This augmentation is carried out with careful and precise control of transformations that are dependent on the presence of tungsten. The objective is to deliberately prevent polyphasic grain growth, where multiple phases or structures develop within the alloy, particularly during critical manufacturing processes such as sintering and solid-state fusion. The meticulous regulation of these transformations is crucial for achieving the desired microstructure and, consequently, improving the overall mechanical performance of the tungsten-based alloy [8, 13].

Significantly, the incorporation of TiC particles notably restrains tungsten particle dissolution and precipitation within the liquid copper phase, curtailing phase growth during sintering [17, 28]. The exploration of TiC incorporation at varied concentrations aims to achieve a microstructure with finely distributed γ-Cu bonding phases, leading to pronounced enhancements in mechanical properties [19, 11], demonstrating remarkable thermal stability at elevated temperatures and mitigating grain growth within the tungsten component [16].

This study is dedicated to a comprehensive exploration of TiC's impact on the mechanical properties and microstructure of W-Cu-TiC alloys, intending to unravel the intricacies of densification, sintering behavior, and strengthening within the domain of TiC-enriched W-Cu alloys [9, 24].

2. MATERIALS AND MATHEMATICAL FORMULATION

The experimentation involved the utilization of tungsten (W), copper (Cu), and titanium carbide (TiC) powders with a particle size ranging from 38 to 50 micrometers and approximately 99% purity, following established protocol [12]. A meticulous preparation process commenced with high-energy ball milling of sample blends at a rotation speed of 950 rpm for an 8-hour duration. Subsequently, these blends underwent cold uniaxial compaction at a pressure of 30 MPa [18, 20].

The resultant powder mixture, encompassing 20 g of the composite, was then compressed at a pressure of 30 MPa, yielding cylindrical pellets measuring Ø15 mm in diameter and 10 mm in thickness. Moreover, (3555) mm specimens were fashioned specifically for flexural testing [15, 1]. Density measurements were conducted both pre- and post-sintering using a digital densimeter Voyager Pro (VP6102C). The samples underwent sintering in a hydrogen sintering furnace equipped with a resistance filament, employing a constant heating rate of 5 °C/min. Sintering transpired over a two-hour period at a temperature of 1200°C [21].

The microstructural alterations were scrutinized using a scanning electron microscope (SEM), the JEOL JSM-6063 model, while computer-assisted microhardness measurements were executed employing an AFFRI-DM2D hardness tester. Furthermore, flexural testing was performed utilizing the WE-10K universal hydraulic testing machine. The determination of various phases present in the samples was facilitated by employing a PHILIPS diffractometer. These comprehensive experimental procedures provided critical insights into the microstructural changes, mechanical properties, and phase compositions of the synthesized W-Cu-TiC alloys [22].

3. RESULTS AND DISCUSSION

SEM analysis revealed evolving morphological features of WCuTiC alloys with varying Titanium Carbide (TiC) proportions. Post-sintering SEM images displayed uniformity, corroborated by density measurements. Phases included a tungsten-copper matrix integrated with TiC particles, showing diverse carbon bonding arrangements with tungsten facets. XRD analysis identified predominant tungsten phases, copper, and TiC, showcasing a phase evolution with increased TiC content, emphasized by intensified TiC peaks.

Mechanical tests unveiled TiC's influence: hardness improved linearly with TiC content, reaching 1273 HV0.1 at 15%, while flexural strength peaked at 1745 N/mm². Density rose with sintering temperature and TiC content, hitting 13.8 g/cm³ at 15%. Excessive TiC aggregation adversely affected performance. These results underscore TiC's significance in structurally and mechanically shaping WCuTiC alloys.

3.1. Scanning Electron Microscope SEM Analysis

The SEM analysis presented in Figure 3.1. delineates the morphological progression of WCuTiC alloys characterized by varying Titanium Carbide (TiC) proportions. Notably, the absence of pores attests to the homogeneity achieved during the sintering process, a finding corroborated by density measurements. The recorded densities for the respective TiC proportions of 5%, 10%, and 15% stand at 9.60 g/cm³, 11.40 g/cm³, and 13.80 g/cm³. The sintered tungsten and copper alloy, W30Cu, exhibits a discernible solid matrix, while the identification of TiC presents a more intricate analysis.

Figures 3.1a, 3.1b, and 3.1c, acquired via SEM imaging of sintered samples containing 5%, 10%, and 15% TiC, unveil distinct features within the microstructures. The white coloring denotes copper particles serving as binders, gray areas represent various tungsten phases, and dark gray TiC particles are observed in limited quantities. The presence of TiC particles fluctuates with the TiC content due to carbon's varied bonding with distinct tungsten facets.

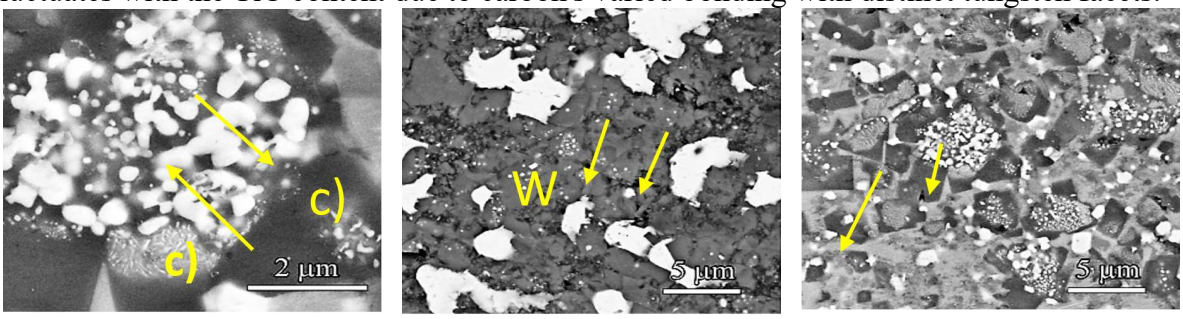

(a) (b) (c)

Fig. 3.1. SEM image by backscattered electrons of samples with different TiC proportions, (a) x=5%, (b) x=10%, (c) x=15% of TiC

Figure 3.1a illustrates the surface micrograph of a sample with 5% Titanium Carbide (TiC), revealing black spots—identified by yellow arrows—attributed to Tungsten Cabride (WC) contamination during sintering. The 10% TiC sample displays varied distribution of TiC particles within the microstructure, yet achieving uniform dispersion is challenging, notably at

higher TiC contents, with 10% and 15% by weight, due to tungsten particle aggregation. Agglomeration results in elongated conglomerates and persists even after sintering, indicating the stability of WC particles.

The distribution of TiC particles by weight between 5% and 10% accentuates solid phase growth effects, evidencing the diffusion of carbide particles into the tungsten matrix and forming larger WC particles. Notably, decarburization of TiC particles is more pronounced in samples with 15% TiC. XRD patterns affirm TiC diffusion into the tungsten matrix, forming solid solutions, corroborating earlier discussions. The growth and aggregation of TiC particles are observed notably in samples with 5% and 10% TiC, with larger conglomerates formed post-sintering for the 15% TiC sample.

3.2. X-ray Diffraction (XRD) Analysis

The XRD analysis, a standard technique for identifying crystalline phases within an alloy, divulges critical insights into the chemical composition of the W-Cu-TiC alloy reinforced with varying TiC proportions (5%, 10%, and 15% by weight). Figures 3.2a, 3.2b, and 3.2c elucidate the XRD diffraction patterns, delineating distinct characteristics for each composition.

The positioning of peaks primarily suggests the dominance of tungsten (W) within the alloy. In addition to W, the distinct presence of copper (Cu) and titanium carbide (TiC) is evident across all XRD patterns. Figure 3.2a emphasizes the presence of W and W2C phases in the sintered W powders. Notably, the XRD analysis in Figure 3.2b reveals peaks corresponding to (Ti, W) alongside base phases such as W, W2C, and a solid solution of 30Cu.

Remarkably, the intensity of Cu-associated peaks diminishes as the weight percentage of TiC increases (Figure 3.2c). This decline in Cu intensity suggests a controlled sintering environment, limiting the formation of undesired oxides.

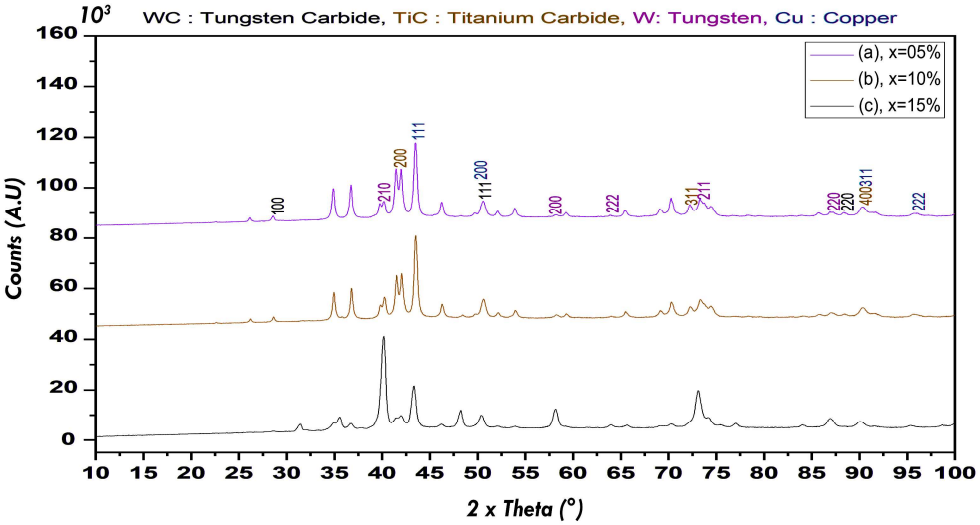

Fig. 3.2. Phase analysis by XRD of TiC

The XRD patterns further emphasize the augmentation of TiC-associated peaks with increasing proportions of reinforcing particles. This emphasizes the presence of Cu particles within the W matrix. Additionally, the analysis highlights a consistent amount of Cu across all samples, evidenced by peaks of similar intensity. However, the intensity of TiC-related peaks notably escalates with the rise in TiC content from 5% to 15% by weight. This observation signifies the proportional increase in TiC particles within the alloy matrix, underlining the impact of TiC content variation on the XRD patterns and the consequent phase composition changes within the alloy.

The densification resulting from sintering reduces pores in the microstructure at 1200°C, as noted in Figure 3.3 (highlighted by red arrows). This reduction in porosity positively influences the superior mechanical properties observed.

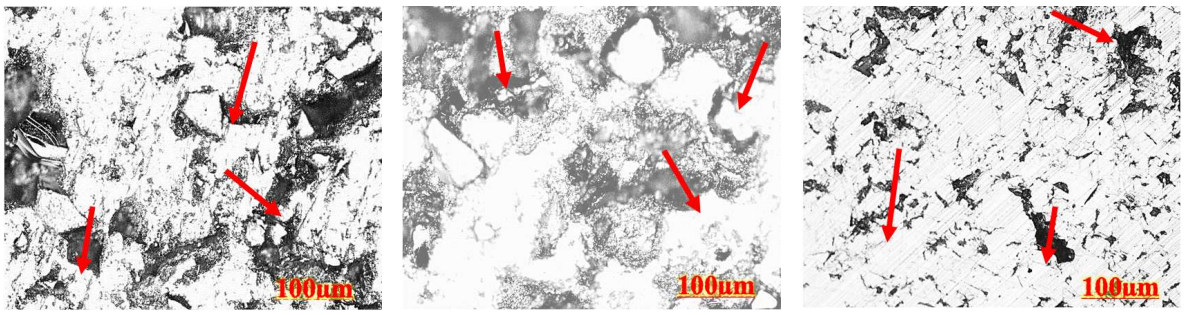

(a) (b) (c)

Fig. 3.3. Scanning electron microscopy OM image of porosity,
(a) x=5%, (b) x=10%, (c) x=15% of TiC

3.3. Effect of TiC on Hardness

The microhardness analysis of the WCuTiC alloy in Figure 3.4 displays a discernible and consistent enhancement in microhardness values, spanning from 871 to 1273 HV0.1, concomitant with the augmentation of TiC content. The rise in microhardness reaches its peak, approximately 1273 HV0.1, at a concentration of 15% by weight of TiC. Comparatively, microhardness values of 871 HV0.1 were recorded for 5% by weight of TiC, and 1024 HV0.1 for the sample with 10% by weight of TiC.

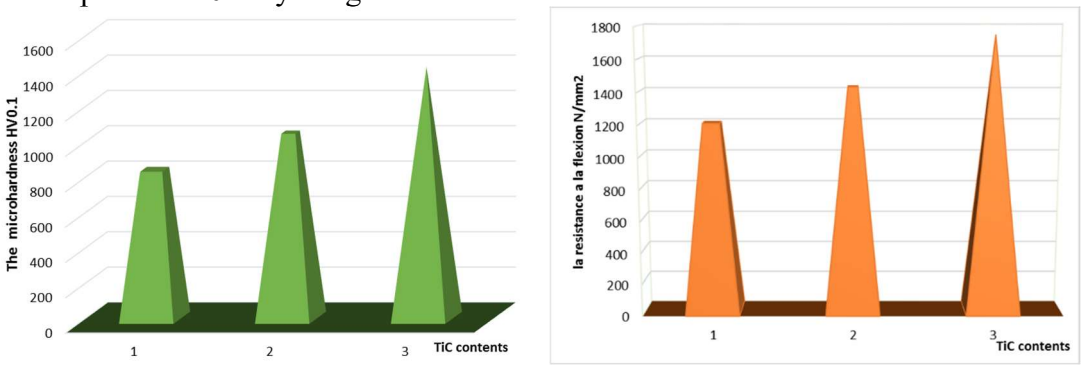

(a) (b)

Fig. 3.4. .The evolution, (a) microhardness, (b) flexural strength

This increase in microhardness can be attributed to the well-dispersed TiC reinforcement particles within the tough phase.

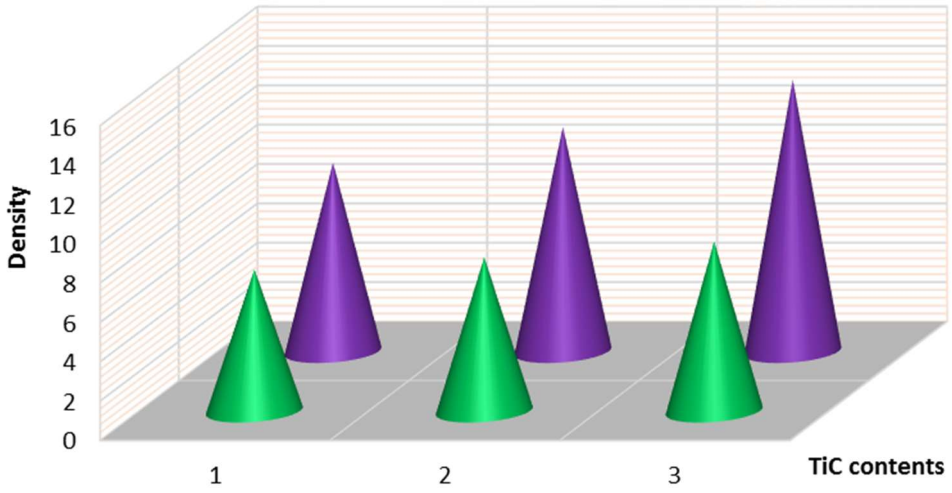

Fig. 3.5. .Density evolution before and after sintering

The precision in conducting microhardness tests ensured the positioning of the indenter precisely within areas where both W and TiC particles are present (Figure 3.6a, 3.6b, and 3.6c).

The integration of hard ceramic particles within the alloys enriched dislocations, a pivotal factor contributing to the observed peak microhardness in samples featuring a higher concentration of reinforcement.

The reinforcement's contribution to enhancing microhardness lies in the enrichment of dislocations within the alloys. The integration of hard ceramic particles like TiC curtails the energy of grain boundaries, impedes their mobility, and obstructs dislocation movement. This impediment preserves the size of tungsten particles and stabilizes TiC grain size during sintering, ultimately resulting in escalated microhardness.

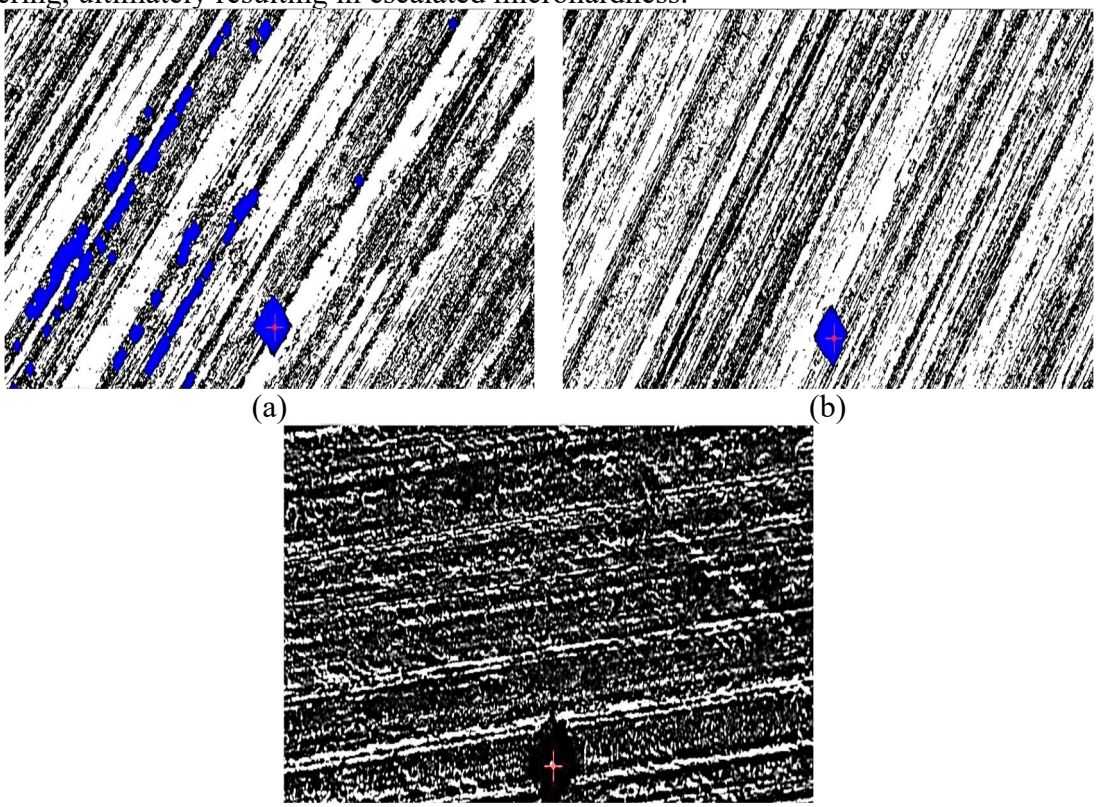

Fig. 3.6. Microhardness impression and values,
(a) x=5%, (b) x=10%, (c) x=15% of TiC

Additionally, the improved microhardness, owing to reinforcement addition, can also be attributed to the higher hardness of Cu and TiC particles in comparison to the ductile tungsten alloy matrix. The hardness superiority of these reinforcement particles significantly contributes to the overall enhancement in microhardness observed in the composite alloy.

Table 3.1 presents the measured values for Hardness (HV), Diagonal X, Diagonal Y, and Force (gf) for the respective cases (a), (b), and (c), aligned with varying TiC content percentages.

Table 3.1 Indentation measurement result

Case	Hardness (HV)	Diagonal X (Microns)	Diagonal Y (Microns)	Force (gf)
Case (a), x=05%	871	47.9	44.3	1000
Case (b), x=10%	1024	41.6	43.6	1000
Case (c), x=15%	1273	39.2	37.2	1000

3.4. Effect of TiC on Flexural Strength

Figure 4b delineates the flexural strength of samples featuring various weight proportions of TiC particles, indicating a discernible rise in flexural strength as TiC content within the

tungsten-copper alloy matrix increases. The graph demonstrates that alloys integrating 15% TiC particles display notably elevated flexural strength compared to samples with 5% and 10% TiC. Initially, samples with 5% TiC showcased a flexural strength of 1200 N, significantly elevating to 1745 N/mm² with 15% TiC, attributing this enhancement directly to the addition of TiC. Comparatively, the W-Cu-15% TiC alloy experienced a remarkable 26% increment in flexural strength.

The observed strength improvement can be attributed to various factors. Primarily, the interfaces between copper and TiC create substantial multidirectional thermal stresses, fortifying the alloy's structure. Additionally, the refinement of the crystalline structure contributes significantly to enhanced alloy strength. The robust bond between the W-Cu alloy matrix and TiC particles, along with their uniform distribution, emerge as pivotal elements fostering increased flexural strength in composites (Figure 6a, b, and c).

Moreover, the integration of TiC particles restricts dislocation mobility through dispersion strengthening mechanisms. As the number of TiC particles increases, the reduced distance between them necessitates more force to move dislocations through these particles. The resultant increase in composite strength is directly associated with this modification.

These findings align with the established advantages of using powder metallurgy processes for manufacturing alloys, facilitating uniform grain distribution and robust bonding between phases, particularly enhancing composite sample strength through TiC addition to the WCu matrix. The observed strength increase can also be attributed to microstructural modifications induced by the reinforcement's addition, resulting in a high density of dislocations and significant disparities between the reinforcements and the tungsten matrix.

3.5. Effect of Density

The investigation of density in our study included two pivotal measurements: green density and post-sintering density, denoting the sample density before and after the sintering process. The determination involved measuring the mass and dimensions of the samples employing a caliper.

The initial green density exhibited a progression from 7.2 for 5%, 7.8 for 10%, to 8.6 g/cm³ for 15% TiC. The influence of sintering temperature on density is markedly apparent. Post-sintering, the density highlighted a proportional increase, starting at a minimum of 9.6 for 5%, escalating to 11.4 for 10%, and reaching 13.8 g/cm³ for 15% TiC, as portrayed in Figure 4c.

The green density exhibited a gradual rise commensurate with the increase in TiC content up to 15%, reaching 8.6 when the sintering temperature was adequately high. This rise confirms the cumulative impact of the Cu binder and the complete pore filling between particles.

Moreover, the post-sintering density swiftly ascended to 13.8, nearing the theoretical density, signifying the substantial influence of both sintering temperature and TiC content on the overall density. This observation underscores the critical interplay between TiC content and sintering conditions in shaping the density profile, indicating their pivotal roles in the density enhancement process.

3.6. Effect of Adding TiC on Mechanical Properties

The investigation delved into the impact of integrating TiC at various concentrations on the microstructure and mechanical attributes. Addition of fine TiC particles, exhibiting an average size, led to their cohesion around W particles, thereby enhancing interfacial bonding strength, wear resistance, and microhardness.

The TiC grains' distributed and uniform shape, as depicted in Figure 6 (in the yellow rectangle), wielded a positive influence, culminating in the attainment of essential mechanical properties crucial in industrial applications, particularly in addressing wear and corrosion issues across diverse uses. Nonetheless, excessive TiC aggregation markedly compromised the overall performance. Among the tested WCuTiC samples, those harboring 15% TiC by weight

showcased superior performance metrics, boasting an average microhardness of 1273±5 HV0.1, a flexural strength of 1745 N·mm², and a post-sintering density of 13.8 g/cm³, with uniform microstructures (Figure 6a, b, and c).

This study unequivocally demonstrates the applicability of the solid-state sintering method in alloy preparation, offering a promising path for further explorations in the domain of sintered alloy fabrication. The outcomes highlight the critical balance required in TiC integration, emphasizing the necessity to avoid excessive TiC aggregation to preserve and enhance the desirable mechanical attributes within the composite, while also underscoring the pivotal role of TiC distribution and shape in optimizing the overall performance of WCuTiC alloys.

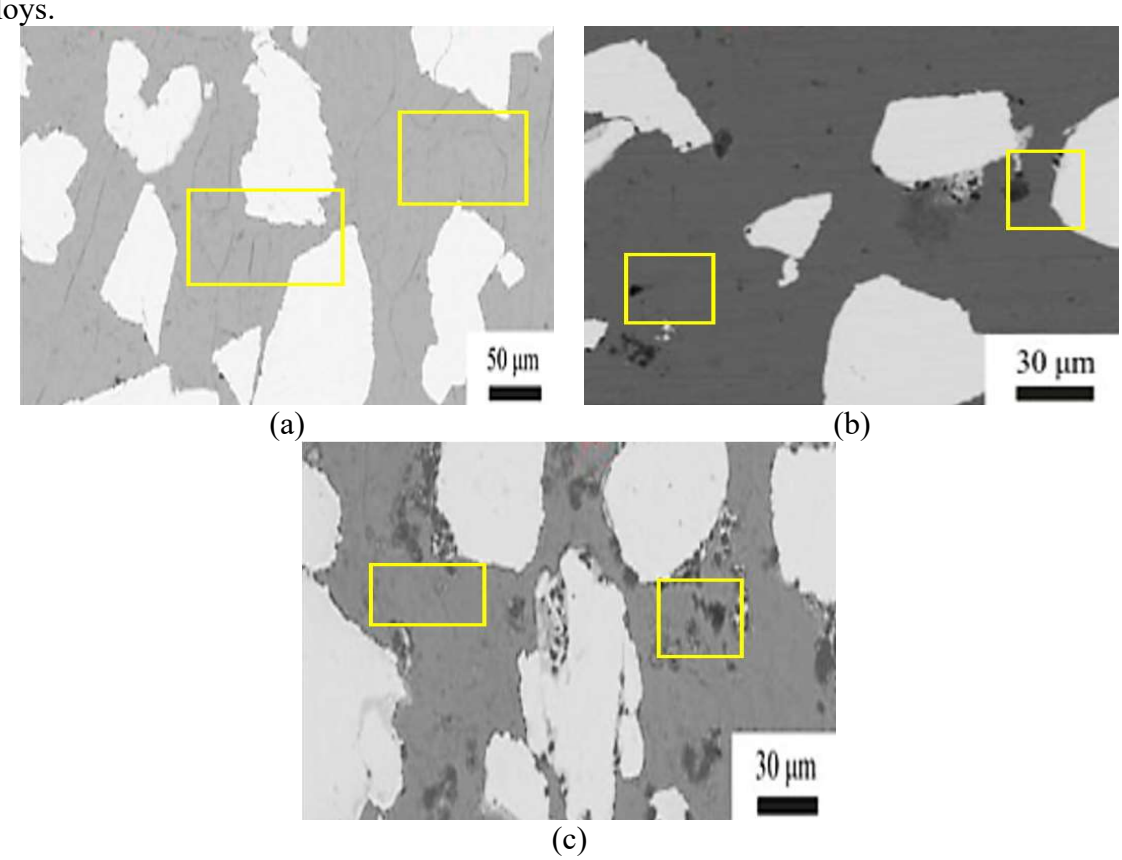

(a) (b)

(c)

Fig. 3.7. SEM image by backscattered electrons of phase,
(a) x=5%, (b) x=10%, (c) x=15% of TiC

4. CONCLUSION

In summary, the successful fabrication of a TiC-reinforced WCu alloy through solid-state sintering using metal powders has demonstrated promising wear resistance properties. While this study specifically focused on the WCu/TiC ratios, it is crucial to acknowledge the potential for other compositions.

The recommended manufacturing process involving grinding, compaction, and sintering at 1200°C proved integral in achieving reduced pore sizes through densification and particle size optimization. The density of WCu/TiC alloys reached 13.8%, and significant porosity reduction was observed in samples containing 15% TiC after a 2-hour sintering period.

Notably, the sample incorporating 15% TiC displayed minimal porosity and highlighted an optimal hardness of approximately 1273 HV0.1. Conversely, samples featuring 5% TiC exhibited relatively lower hardness values, below 900 HV0.1. This alloy exhibited improved mechanical attributes alongside enhanced flexural strength, rendering it suitable for various application areas, aligning with the study's initial expectations.

The performance of TIC-W-Cu alloy in real-world applications can be influenced by various external factors, including temperature and environmental conditions. TIC-W-Cu alloy

may exhibit good performance at high temperatures, as tungsten carbide (WC) is known for its high melting point and hardness. However, the copper (Cu) component has a lower melting point, so extreme temperatures might affect the overall stability of the alloy.

Tungsten and copper have different coefficients of thermal expansion. This can lead to internal stresses within the alloy when exposed to temperature variations. These stresses may affect the structural integrity of the alloy over time. The presence of aggressive chemicals in the environment can influence the alloy's performance. Copper is susceptible to corrosion, and the corrosive nature of the environment may affect the overall integrity of the alloy. TIC-W-Cu alloys are often used in applications requiring high wear resistance. The alloy's performance can be influenced by the type and intensity of mechanical loading. Extreme impact or abrasion can lead to wear and degradation over time. The manufacturing process, especially the sintering conditions, can affect the microstructure and properties of the alloy. Proper control of these parameters is crucial for achieving desired performance.

Nevertheless, practical assessments under real operational conditions are crucial to provide concrete insights into potential technical challenges that may arise in industrial settings. These evaluations would further validate the alloy's performance and durability, offering invaluable insights for its industrial implementation.

REFERENCES

1. Boukhobza, A., Fedaoui, K., Mebarki, L., Arar, K. & Baroura, L. (2021). Compaction and heat treatment effects on the structural and mechanical properties of sintered Fe3C-W-co alloys, *International Journal of Engineering Research in Africa*, **52**, 1–10, https://doi.org/10.4028/www.scientific.net/jera.52.1
2. Dong, L., Chen, W., Zheng, C. & Deng, N. (2017). Microstructure and properties characterization of tungsten–copper composite materials doped with graphene, *Journal of Alloys and Compounds*, **695**, 1637–1646, https://doi.org/10.1016/j.jallcom.2016.10.310
3. Liu, J., Liu, J., Wang, X., Fu, C., Wang, Y., et al. (2021). Phase-transformation dynamics and characterization of precipitates in the Cu-3Ti-3ni-0.5Si Alloy, *Materiali in Tehnologije*, **55**(4), https://doi.org/10.17222/mit.2020.166
4. Liu, J., Wang, X., Liu, J., Li, H., Liang, Y., et al. (2021). Influence of copper powder morphology on the microstructure and properties of copper matrix bulk composites reinforced with ni-doped graphene, *Archives of Metallurgy and Materials*, 341–348, https://doi.org/10.24425/amm.2022.137764
5. Mebarki, L., Zidani, M., Boukhobza, A., Mechachti, S. & Fedaoui, K. (2018). Effect of the proportion of tungsten element on the mechanical and structural properties of (fe3C-W-ni) sintered alloy, *Diffusion Foundations*, **18**, 35–40, https://doi.org/10.4028/www.scientific.net/df.18.35
6. Memisoglu, G., Gulbahar, B. & Varlikli, C. (2021). Applications of graphene-based composite materials, *Composite Materials*, 173–198, https://doi.org/10.1201/9781003080633-10
7. Naseer, A., Ahmad, F., Ali, S. & Haider, W. (2022). Powder injection molded nano copper oxide grafted graphene reinforced copper matrix composites, *Powder Technology*, **397**, 117101, https://doi.org/10.1016/j.powtec.2021.117101
8. Xie, H., Guan, W., Lv, H., Yang, H., Gao, M., et al. (2022). W–Cu/CU composite electrodes fabricated via laser surface alloying, *Materials Characterization*, **185**, 111715, https://doi.org/10.1016/j.matchar.2021.111715
9. Yan, A., Wang, Z., Yang, T., Wang, Y. & Ma, Z. (2016). Microstructure, thermal physical property and surface morphology of W-cu composite fabricated via Selective Laser Melting, *Materials & Design*, **109**, 79–87, https://doi.org/10.1016/j.matdes.2016.07.049
10. Zhou, H., Feng, K. & Liu, Y. (2022). Densification, microstructure, and properties of W-mo-cu alloys prepared with nano-sized cu powders via Large Electric Current Sintering, *Advanced Powder Technology*, **33**(8), 103703, https://doi.org/10.1016/j.apt.2022.103703
11. Al-Sayed, S. R., Elgazzar, H. & Nofal, A. (2022). Microstructure evaluation and high-temperature wear performance of hard protective layer deposited on titanium alloy via laser metal deposition, *Metals and Materials International*, **28**(11), 2822–2835,

https://doi.org/10.1007/s12540-021-01160-x
12. Ananthi, N., Elaiyarasan, U., Satheeshkumar, V., Senthilkumar, C., & Sathiyamurthy, S. (2022). Effect of WC–cu composite electrodes on material deposition rate, microhardness and microstructure of electrical discharge coated magnesium alloy, *Surface Review and Letters*, **29**(04), https://doi.org/10.1142/s0218625x22500500
13. Chen, Q., Li, L., Man, X., Sui, H., Liu, J., et al. (2021). In-situ synthesis of Core-Shell Structure W(WC) composite grains in W-cu composites fabricated by infiltration, *Journal of Alloys and Compounds*, **864**, 158633, https://doi.org/10.1016/j.jallcom.2021.158633
14. Deng, N., Zhou, Z., Li, J. & Wu, Y. (2019). W–cu composites with homogenous Cu–network structure prepared by Spark Plasma Sintering using core–shell powders, *International Journal of Refractory Metals and Hard Materials*, **82**, 310–316, https://doi.org/10.1016/j.ijrmhm.2019.05.003
15. Kim, S., Park, S.-Y., Lim, J.-B., Kwon, S. H. & Lee, K.-A. (2023). Effect of WC particle size on the microstructure, mechanical and electrical properties of AG/WC Sintered Electrical Contact material, *Journal of Korean Powder Metallurgy Institute*, **30**(3), 242–248, https://doi.org/10.4150/kpmi.2023.30.3.242
16. Liu, J., Wang, X., Liu, J., Li, H., Liang, Y., et al. (2021). Influence of copper powder morphology on the microstructure and properties of copper matrix bulk composites reinforced with ni-doped graphene, *Archives of Metallurgy and Materials*, 341–348, https://doi.org/10.24425/amm.2022.137764
17. Mebarki, L., Zidani, M., Mechachti, S., Farh, H. & Miroud, D. (2017). Effect of nickel addition study on the mechanical properties of the (fe3C-ni) alloy obtained by solid phase compaction and Sintering, *International Journal of Engineering Research in Africa*, **32**, 18–24, https://doi.org/10.4028/www.scientific.net/jera.32.18
18. Naghikhani, M., Ardestani, M., & Moazami-Goudarzi, M. (2019). Microstructure, mechanical properties and wear performance of WC/Brass Composites produced by pressureless and Spark Plasma Sintering Processes, *Metals and Materials International*, **27**(6), 1639–1648, https://doi.org/10.1007/s12540-019-00564-0
19. Yang, Q., Lu, C., Han, Y., Chen, X., Yang, J., et al. (2022). Influence of cu/W interfacial structure on the resistance against harmful helium atoms: A mechanism analysis, *Journal of Alloys and Compounds*, **903**, 163817, https://doi.org/10.1016/j.jallcom.2022.163817
20. Zhang, M., Yang, K., Wei, G., Xie, W., Yang, Y., et al. (2023). AZ31/GNP Magnesium Composites with Excellent Comprehensive Mechanical Properties Prepared by Friction Stir Processing and Rolling, *Journal of Materials Research and Technology*, **25**, 3078–3092, https://doi.org/10.2139/ssrn.4436207
21. Abderrazak, T. A., Iliace, A., Sofiane, B. M., Ilyas, B. R., Hichem, H., et al. (2023). Enhancing frequency system damping efficiency via optimal integration of VRE in grid. *Proc. of 2023 Second International Conference on Energy Transition and Security (ICETS)* (Kirkuk, Iraq), 1–6, https://doi.org/10.1109/icets60996.2023.10410747
22. Bao, W., Chen, J. & Xie, G. (2022). Optimized strength and conductivity of multi-scale copper alloy/metallic glass composites tuned by a one-step spark plasma sintering (SPS) process, *Journal of Materials Science & Technology*, **128**, 22–30, https://doi.org/10.1016/j.jmst.2022.04.024
23. Chen, W., Chen, P., Li, J., Zhang, J., Luo, L., et al. (2019). Functionally graded W-cu materials prepared from Cu-coated w powders by Microwave Sintering, *Journal of Materials Engineering and Performance*, **28**(10), 6135–6144, https://doi.org/10.1007/s11665-019-04321-7
24. Han, T., Hou, C., Zhao, Z., Huang, X., Tang, F., et al. (2022). W–cu composites with excellent comprehensive properties, *Composites Part B: Engineering*, **233**, 109664, https://doi.org/10.1016/j.compositesb.2022.109664
25. Jiang, Y., Wu, J., Li, Q., Zhu, L. & Wang, X. (2021). Influence of metal vapor on post-arc breakdown for intermediate frequency vacuum arc, *Vacuum*, **193**, 110551, https://doi.org/10.1016/j.vacuum.2021.110551
26. Tian, W., Cao, Y. & Wang, L. (2023). Effect of two-stage solution on microstructure and mechanical property of IN718 alloy fabricated by selective laser melting, *Materials Research Express*, **10**(2), 026520, https://doi.org/10.1088/2053-1591/acbc0b
27. Yang, X., Zhao, Y., Kang, D., Zou, J., Xiao, P. & Liang, S. (2020). The vacuum breakdown properties and arc erosion behaviors of Cutiw alloys, *Engineering Failure Analysis*, **118**, 104865, https://doi.org/10.1016/j.engfailanal.2020.104865

28. Zhang, S., Zhu, Q., Li, Q., Ji, W., Wang, W., et al. (2022). Ultrafine-grained tungsten heavy alloy prepared by high-pressure Spark Plasma Sintering, *Materials*, **15**(17), 6168. https://doi.org/10.3390/ma15176168

